THE APPRAISAL OF NOAA SATELLITES LST-SW ALGORITHMS: NOAA-20 (JPSS-1) PROPOSAL

Nisrine Chekroun

PhD Student, Telecommunication Department, Abdelmalek Essaadi University, Mhannech 2,
Tetouan, Morocco
nisrine.chekroun@gmail.com

Naoufal Raissouni

Professor, RS&GIS, Mhannech 2,
Tetouan, Morocco
naoufal.raissouni.ensa@gmail.com

Mohammed Lahraoua

Professor, GéoTéCa, Boukhalef,
Tangier, Morocco
m_lahraoua@yahoo.fr

Fatima Zahrae Rhziel

PhD Student, RS&GIS, Mhannech 2,
Tetouan, Morocco
96rhzielfatimazahrae@gmail.com

Assaad El Makhloufi

Dr. Eng, RS&GIS, Mhannech 2
assaadelmakhloufi@gmail.com

Abstract

The Split-Window (SW) algorithm has been developed in order to retrieve Land Surface Temperatures (LST) from Thermal InfraRed (TIR) remote sensing data. In this paper, astudy has been carried out using MODTRAN 4.0 radiative transfer code simulations using the TIR channels of the Infrared Imager Radiometer Suite (VIIRS) and The Advanced Very High Resolution Radiometer (AVHRR) onboard the National Oceanic and Atmospheric Administration (NOAA) Satellites to obtain numericalcoefficients of the proposed algorithms. Results fromvalidation, using the standard atmospheric simulation forvarious situations and the ground truth data sets demonstratethe applicability of the algorithm.

A detailed analysis of the estimated total error in LST- SW, $\delta_{Total(Ts)}$, shows that the algorithms are able to estimate accurate LST with mean value of about 1.31 K, a minimum of 1.25 K and a maximum of 1.38 K (with an amplitude of 0.13 K), a standard deviation of about 0.04 K and a root mean square error (rmse) of about 1.31 K.

Keywords: **VIIRS/JPSS-1 (NOAA-20), AVHRR/NOAA satellites, LST-SW, MODTRAN**

1. Introduction

Land Surface Temperature (LST) is one of the keyparameters in the physics of land surface processes [1-5]. The inversion of LST from satellite data requires atmosphere-induced effects correction, mainly the absorption and emission of atmospheric surface emissivity and water vapor [6-21]. Surface emissivity is critical for determining land surface thermal radiation. Variations inatmospheric transmittance strongly depend on the dynamics of water vapor content in the atmospherics profile for thermal channels. The atmospheric water vapor content can be estimated directly from NOAA thermal channels, and transmittance will be further estimated [16]. In this work, weare comparing the performance of the proposed LST-SW for NOAA-20/JPSS-1 and the NOAA (7, 9, 11, 12, 14, 15, 16, 17, 18, 19) series LST-SW algorithms.

2. LST Split-Window Algorithm

The SW algorithm uses the different atmospheric absorptionbehavior for two thermal infrared channels within the 10 µmand 12.5 µm window region. Many researchers have used this algorithm structure to retrieve land/sea surface temperature. In this paper, the SW algorithm proposed by [39/22] has been used, which takes into account the emissivity and water vapor effects:

$$T_s = T_i + C_1(T_i - T_j) + C_2(T_i - T_j)^2 + C_0 + (C_3 + C_4 W)(1 - \varepsilon) + (C_5 + C_6 W)\Delta\varepsilon \quad (1)$$

T_s is the surface temperature (in K) (LST-SW in hereafter), T_i and T_j are the at sensor brightness temperatures of the different thermal channels (in K), $\varepsilon = (\varepsilon_I + \varepsilon_j) / 2$ and $\Delta\varepsilon = (\varepsilon_i - \varepsilon_j)$ are the mean effective emissivity and the emissivity difference, W is the total atmospheric water vapor (in g/cm2). Finally, C_0 to C_6 are the SW coefficients to bedetermined from simulated data.

3. MODTRAN 4.0 Simulations

MODTRAN 4.0 radiative code is used to calculate the brightness temperatures expected at the AVHRR/NOAA satellites (7, 9, 11, 12, 14, 15, 16, 17, 18, 19) thermal channels 4 and 5 and VIIRS/NOAA-20 (JPSS-1) infrared channels M15 and M16 for different atmospheric situations. The profiles of temperature for these situations were obtained from the radiosoundings extracted neatly from the Television InfraRed Observation Satellite (TIROS) Operational Vertical Sounder (TOVS) Thermodynamic Initial Guess Retrieval (TIGR) database [23-25]. The calculations have been done for a large gradient of temperatures, T-5, T, T+5, T+10, and T+20, (T is the first boundary layer temperature of the atmosphere), five different view angles (0º, 10º, 20º, 30º and 40º), 54 atmospheric water vapor (W) values at nadir (with, Wmin=0.15 g/cm2 and Wmax=4.65 g/cm2), and 100 emissivities of spectral responses of several types of surfaces extracted from the Advanced Spaceborne Thermal Emission Reflection Radiometer (ASTER) spectral library [23-2].
The outputs of applying MODTRAN 4.0 radiative code are values of atmospheric parameters: atmospheric transmittance (τ), atmospheric downwelling radiance (Latm↓) and atmospheric upwelling radiance (Latm↑), obtained by mathematical convolution using filter functions of channels (i = 4, M15) and (j = 4, M16) of NOAA satellites (7, 9, 11, 12, 14, 15, 16, 17, 18, 19, 20/JPSS-1).

4. VIIRS Sensor Abroad JPSS-1 (NOAA-20)

The Visible Infrared Imaging Radiometer Suite (VIIRS) instrument is aboard the NOAA's Joint Polar Satellite System (JPSS) providing global observations that serve as the backbone of both short- and long-term forecasts. JPSS-1 is known as NOAA-20. The VIIRS thermal bands include two split window channels, M15 and M16, used for the LST-SW retrieval as shown in Table I.

VIIRS JPSS-1	Wavelength (µm)	Bandwidth (µm)	Spatial Resolution (m)
M15	10.763	10.26-11.26	750
M16	12.013	11.54-12.49	750

Table 1. VIIRS Split Window band characteristics

5. AVHRR Sensor abroad NOAA satellite series

The Advanced Very High Resolution Radiometer (AVHRR) instrument was carried on so many satellites as TIROS and NOAA series (from NOAA-6 to NOAA-19). IT is the backbone for the 1km global land cover product. AVHRR is a multispectral sensor with six spectral bands.
This includes red, thermal, mid, and near-infrared bands. But over time, their spectral ranges have varied. For example, AVHRR/3 channel characteristics are as follows:

Band	Name	Spectral Range (µm)	Applications
Band 1	Red	0.58-0.68	Urban, vegetation, snow/ice, daytime clouds
Band 2	Near IR	0.725-1.00	Vegetation, land/water boundaries, snow/ice, flooding
Band 3A	Mid IR	1.58-1.64	Vegetation, snow/ice detection, dust monitoring
Band 3B	Thermal	3.55-3.93	Surface temperature, wildfire detection, nighttime clouds, volcanic eruptions
Band 4	Thermal	10.30-11.30	Surface temperature, wildfire detection, nighttime clouds, volcanic eruptions
Band 5	Thermal	11.5-12.50	Sea surface temperature, water vapor path radiance

Table 2. AVHRR band characteristics

The VIIRS/NOAA-20 satellite sensor response function is shown in Figure 1 compared to AVHRR channels 4 and 5.

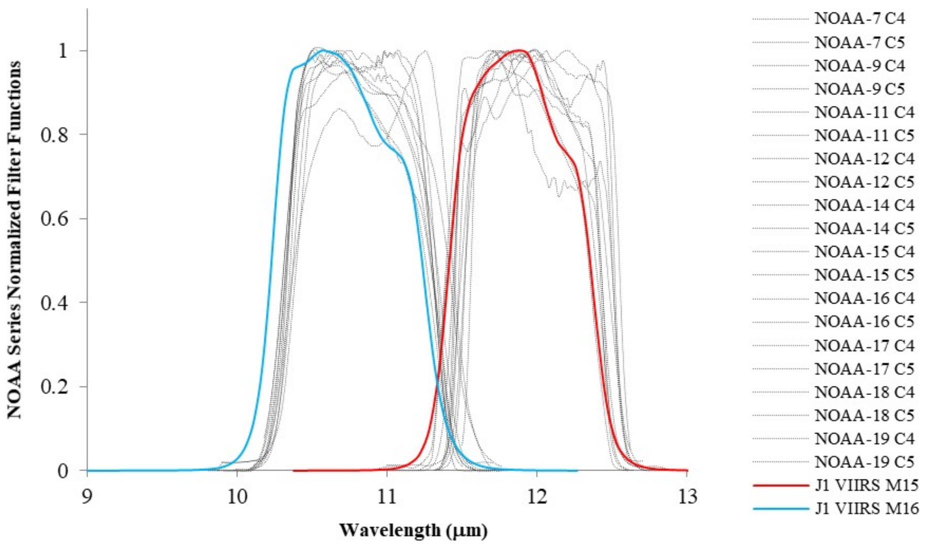

Fig. 1. Normalized filter function of JPSS-1/NOAA-20 VIIRS infrared channels and AVHRR/NOAA satellite series.

6. Sensitivity Analysis

The LST-SW algorithm coefficients C (i = 0, 1, 2, 3, 4, 5, 6) (see Equation (1)) were obtained from the minimization of 135000 simulation data (54 atmospheric profiles, 5 T values, 100 emissivities, 5 view angles) included in the constructed database for the NOAA satellites (7, 9, 11, 12, 14, 15, 16, 17, 18, 19 and 20/JPSS-1). In order to quantify the impact of each error source on the LST-SW algorithm, a sensitivity analysis was carried out in order to examine the performance of the developed methodology under different meteorological conditions and land cover types. Based on the error theory, the following equation has been considered:

$$\delta_{Total}(T_s) = \sqrt{\delta_{alg}^2 + \delta_{NE\Delta E}^2 + \delta_{\varepsilon}^2 + W} \quad (2)$$

where δalg is the standard deviation associated with the algorithm and, $\delta_{NE\Delta T}$ δε and δW are the contribution to the total error due to the uncertainties for at-sensor temperatures, land surface emissivity and atmospheric water vapor, respectively, given by:

$$\delta_{NE\Delta E} = \sqrt{\left(\left|\frac{\partial T_S}{\partial T_4}\right|\right)^2 e^2(T_4) + (\left|\frac{\partial T_S}{\partial T_5}\right|)^2 e^2(T_5)} \quad (3)$$

$$\delta_{\varepsilon} = \sqrt{\left(\left|\frac{\partial T_S}{\partial \varepsilon_4}\right|\right)^2 e^2(\varepsilon_4) + (\left|\frac{\partial T_S}{\partial \varepsilon_5}\right|)^2 e^2(\varepsilon_5)} \quad (4)$$

$$\delta_W = \left|\frac{\partial T_S}{W}\right| e(W) \quad (5)$$

Thus, assuming typical values for the different errors, e(T4, M15) = e(T5, M16) = 0.05 K, e(ε4, εM15) = e(ε5, εM16) = 0.01 = 1% or e(ε4, εM15) = e(ε5, εM16) = 0.005 = 0.5% and e(W) = 0.5 g/cm2.

7. Simulation Results

Table 3 compiles the LST-SW coefficients (C0 to C6) obtained from MODTRAN 4.0 radiative code simulations and regressions that can be used to estimate LST-SW from thermal infrared sensors of NOAA satellites (7, 9, 11, 12, 14, 15, 16, 17, 18, 19, 20/JPSS-1).

NOAA	λ_{ieff}	λ_{jeff}	C 0	C 1	C 2	C 3	C 4	C 5	C 6
7	10.786	11.896	-0.029	1.651	0.292	58.0	-0.32	-118	7.73
9	10.774	11.85	0.072	1.954	0.282	56.8	0.13	-141	11.83
11	10.794	11.891	0.021	1.878	0.268	57.2	0.07	-132	10.31
12	10.857	11.945	0.030	1.623	0.306	57.1	-0.08	-135	12.1
14	10.857	11.982	0.003	1.449	0.261	58.1	-0.33	-115	8.54
15	10.82	11.926	-0.026	1.679	0.295	57.4	-0.14	-126	9.57
16	10.914	11.977	-0.167	1.399	0.305	57.5	-0.18	-150	16.13
17	10.797	11.927	-0.018	1.629	0.286	57.8	-0.23	-121	8.59
18	10.797	12.016	-0.146	1.246	1.234	58.8	-0.49	-107	7.85
19	10.793	12.045	-0.188	1.091	0.218	59.4	-0.67	-100	6.92
20 JPSS-1	10.763	12.013	-0.160	1,331	0.234	58.1	-0.57	-112	8.84

Table 3. LST-SW COEFFICIENTS (C0 TO C6) FOR NOAA SATELLITES (7, 9, 11, 12, 14, 15, 16, 17, 18, 19, 20/JPSS-1)

NOAA	λ_{ieff}	λ_{jeff}	R	δ_{alg} (K)	$\delta_{NE\Delta T}$ (K)	δ_{ε} *(1%)*	δ_{ε} *(0.5%)*	δ_W	δ_{Total} (T_S)	δ_{Total} (T_S)
7	10.786	11.896	0.95	1.05	0.27	1.46	0.73	0.02	1.82	1.31
9	10.774	11.85	0.96	1.04	0.31	1.64	0.82	0.04	1.97	1.36
11	10.794	11.891	0.96	1.04	0.29	1.57	0.79	0.03	1.91	1.34
12	10.857	11.945	0.94	1.06	0.28	1.56	0.78	0.06	1.91	1.35
14	10.857	11.982	0.94	1.06	0.25	1.39	0.7	0.03	1.77	1.29
15	10.82	11.926	0.95	1.05	0.28	1.51	0.76	0.03	1.86	1.33
16	10.914	11.977	0.93	1.07	0.26	1.63	0.82	0.11	1.97	1.38
17	10.797	11.927	0.95	1.05	0.27	1.46	0.73	0.03	1.82	1.31
18	10.797	12.016	0.94	1.07	0.22	1.32	0.66	0.03	1.71	1.28
19	10.793	12.045	0.93	1.07	0.21	1.25	0.63	0.03	1.66	1.25
20 JPSS-1	10.763	12.013	0.91	1.09	0.23	1.35	0.67	0.04	1.75	1.30
		min	0.91	1.04	0.21	1.25	0.63	0.02	1.66	1.25
		max	0.96	1.09	0.31	1.64	0.82	0.11	1.97	1.38
		mean	0.94	1.06	0.27	1.46	0.73	0.03	1.82	1.31
		stdv	0.01	0.02	0.03	0.13	0.07	0.03	0.10	0.04
		rmse	0.94	1.06	0.27	1.47	0.73	0.04	1.82	1.31

Table 4. Sensitivity Analysis: δalg error due to the minimization with the corresponding correlation coefficient ® δNEΔT error due to the noise equivalent Delta Temperature, δε error due to uncertainty of the surface emissivity, δw error due to uncertainty of the atmospheric water vapor content, and δTotal (Ts) the total error in the LST considering typical values of emissivity errors e(εi) = e(εj) = 1 % AND e(εi) = e(εj) = 0.5 %.

Table 4 compiles the corresponding sensitivity analysis for the NOAA satellites. The error due to the minimization, δ_{alg} (in K), with values varying between a minimum of 1.04 K and a maximum of 1.09 K with a correlation coefficient, R, varying between 0.91 and 0.96. The error due to the noise equivalent to delta temperature, $\delta_{NE\Delta T}$, is varying between a minimum of 0.21 K and a maximum of 0.31 K. The error due to the uncertainty of the atmospheric water vapor content, δw, shows variation between a minimum of 0.02 K and a maximum of 0.11 K.
The error due to the uncertainty of the surface emissivity δε, shows variation with a minimum of 1.25 K and a maximum of 1.64 K considering e(εi) = e(εj) = 1 % and variation with a minimum of 0.63 K and a maximum of 0.82 K considering e(εi) = e(εj) = 0.5 %. Finally, the total error in LST, δTotal(Ts), is showing a mean error value of 1.82 K and a variation with a minimum of 1.66 K and a maximum of 1.97 K considering e(εi) = e(εj) = 1 % and a mean error value of 1.31 K with a minimum of 1.25 K and a maximum of 1.38 K considering e(εi) = e(εj)= 0.5 %.
Figure 2 shows that the LST-SW algorithms are able to produce LST NOAA series with values of root mean square error (rmse = 1.82 K) and standard deviation (stdv = 0.10 K) considering e(εi) = e(εj)= 1 %, and (rmse = 1.31 K; stdv = 0.04 K) considering e(εi) = e(εj)= 0.5 %. The totality of the LST-SW algorithms present high correlation values between 0.91 and 0.96.

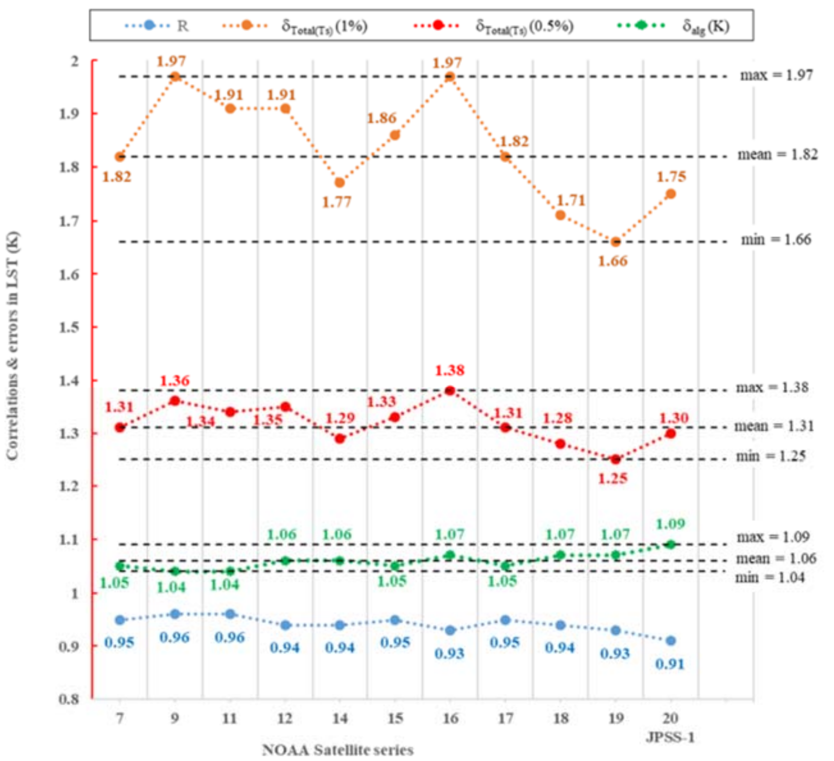

Fig. 2. Parameters representation

8. Validation

Validation is necessary in order to understand how well the retrieved LST with the algorithm matches the actual one in the real world.
In this section, we aim to validate the proposed Split-Window (SW) algorithms for NOAA-11 and 12 using Hay and Walpeup in situ measurements data and to study the behavior of the pseudo-validation of SW algorithms for NOAA (7, 9, 14, 15, 16, 17, 18, 19), NOAA-20 RL, NOAA-20 Enterprise and JPSS-1/ NOAA-20. General statistics: Minimum (Min). Maximum (Max). Average (μ) and Standard deviation (σ). The effective wavelengths

λieff (µm) and λjeff (µm) for the SW AVHRR Channel 4 and 5. The effective wavelength difference between AVHRR Channel 4 and Channel 5: Δλ = λ5eff - λ4eff µm. Mean differences (bias) (K). Standard deviation of differences (K). Root Mean Square Error (K)

Sensor	**Sites**	**λieff (µm)**	**λjeff (µm)**	**Δλ (µm)**	**Mean differences (bias) (K)**	**Standard deviation of differences (K)**	**Root Mean Square Error (K)**
NOAA-7	Hay and Walpeup (NOAA-11)	10.79	11.9	1.11	0,78	1,45	1,65
NOAA-9		10.77	11.85	1.08	0,55	1,56	1,66
NOAA-11		10.79	11.89	1.10	0,65	1,52	1,65
NOAA-12		10.86	11.95	1.09	0,70	1,45	1,61
NOAA-14		10.81	11.98	1.17	0,86	1,39	1,63
NOAA-15		10.82	11.93	1.11	0,76	1,46	1,65
NOAA-16		10.91	11.98	1.06	0,93	1,40	1,68
NOAA-17		10.80	11.93	1.13	0,78	1,44	1,64
NOAA-18		10.80	12.02	1.22	1,11	1,36	1,76
NOAA-19		10.79	12.04	1.25	1,23	1,37	1,84
JPSS-1/NOAA-20		10.70	12.05	1.35	1,11	1,37	1,76
NOAA-7	Hay and Walpeup (NOAA-12)	10.79	11.9	1.11	1,17	1,19	1,66
NOAA-9		10.77	11.85	1.08	1,00	1,26	1,61
NOAA-11		10.79	11.89	1.10	1,08	1,24	1,64
NOAA-12		10.86	11.95	1.09	1,09	1,17	1,60
NOAA-14		10.81	11.98	1.17	1,18	1,14	1,64
NOAA-15		10.82	11.93	1.11	1,15	1,19	1,66
NOAA-16		10.91	11.98	1.06	1,29	1,11	1,70
NOAA-17		10.80	11.93	1.13	1,16	1,18	1,65
NOAA-18		10.80	12.02	1.22	1,37	1,11	1,76
NOAA-19		10.79	12.04	1.25	1,44	1,09	1,81
JPSS-1/NOAA-20		10.70	12.05	1.35	1,38	1,11	1,78

Table 5. Validation of the proposed Split-Window (SW) algorithms for NOAA-11 and 12 using Hay and Walpeup in situ measurements data.

In order to give an idea of the approximated behavior of the proposed SW algorithms, we have used this database. Table 5 gives the validation Root Mean Square Error (RMSE) of NOAA algorithms series for the ground truth data set and the third column shows the RMSE of the algorithms for the total measurements of the Hay and Walpeup sites.

The results show that the algorithms are able to produce LST NOAA series with Mean differences between 0.55 K and 1.34 K for Hay and Walpeup (NOAA-11) and 1 K and 1.51 K for Hay and Walpeup (NOAA-12). In addition, the algorithms permit to provide the LST with standard deviation lower than 1.56 K and lower than 1.33 K for the two sites Hay and Walpeup (NOAA-11) and Hay and Walpeup (NOAA-12) respectively.

The validation analysis results that, the algorithms have the ability to produce LST with, RMSE with values varying between 1.61 K and 1.96 K for Hay and Walpeup (NOAA11) and 1.61 K and 2.02 K for Hay and Walpeup (NOAA12) dataset.

Based in total results we conclude that the JPSS-1/NOAA-20 algorithm can be calculate the LST with a bias lower 1,17 K and a Standard deviation of differences of 1,37 K and a RMSE lower than 1.81 K for the total measurements of the Hay and Walpeup sites, which confirms the accuracy of these two algorithms in LST retrieval.

These values are in the range of the algorithm error, and therefore, they give confidence about the performance of the JPSS-1/NOAA-20 LST SW algorithm retrieving from NOAA satellites series data.

9. Conclusion

The good performance of the JPSS-1/NOAA-20 algorithms in validation using data sets indicates that this algorithm is able to provide an accurate LST retrieval in the known atmospheric transmittance and ground emissivity and atmospheric water vapor conditions. The accuracy in LST estimation confirms that this algorithm is a better alternative, in general, for applications to the real LST retrieval from VIIRS sensors data.

References

[1] Borel C., 29 (2008). Error analysis for a temperature and emissivity retrieval algorithm for hyperspectral imaging data International Journal of Remote Sensing, pp. 5029-5045
[2] Duan S. B., *et al.*, (2019). Radiance-based validation of land surface temperature products derived from Collection 6 MODIS thermal infrared data. International Journal of Applied Earth Observation and Geoinformation. Pages 84-92
[3] Du D., *et al.*, (2015). A Practical Split-Window Algorithm for Estimating Land Surface Temperature from Landsat 8 Data. Remote Sens.
[4] Garajeh M. K., *et al.*, (2020)Evaluating the types of split window algorithms for calculating the land surface temperature to determine the best algorithm for MODIS sensor images. Journal of Remote Sensing for Natural Resources. Pages 106-127
[5] Guillevic P. C., *et al.*, (2014). Validation of Land Surface Temperature products derived from the Visible Infrared Imaging Radiometer Suite (VIIRS) using ground-based and heritage satellite measurements. Remote Sensing of Environment. Pages 19-37
[6] Jiménez-Muñoz J.C., *et al.*, 103 (2006). Improved land surface emissivities over agricultural areas using ASTER NDVI. Remote Sensing of Environment, pp. 474-487
[7] Jonasson O., *et al.*, (2022). JPSS VIIRS SST Reanalysis Version 3. *Remote Sens.*
[8] Liu Y., *et al.*, (2019): Enterprise LST Algorithm Development and Its Evaluation with NOAA 20 Data. Remote Sens.
[9] Li H., *et al.*, (2014). Evaluation of the VIIRS and MODIS LST products in an arid area of Northwest China. Remote Sensing of Environment Pages 111-121
[10] Li Z.-L., Becker F. 43 (1993). Feasibility of land surface temperature and emissivity determination from AVHRR data. Remote Sensing of Environment, pp. 67-85
[11] Li Z.-L., *et al.*, (2013). Satellite-derived land surface temperature: Current status and perspectives. Remote Sensing of Environment. Pages 14-37
[12] Moghaddam Y. J., *et al.*, (2015). A Split-Window Algorithm for Estimating LST from Landsat-8 Satellite Images. Journal of Geomatics Science and Technology.
[13] Price J.C., 1984. Land surface temperature measurements from the split window channels of the NOAA-7/AVHRR. *J. Geophys. Res.,* pp. 7231–7237.
[14] Raissouni N. Split-Window LST Algorithms Estimation From AVHRR/NOAA Satellites (7, 9, 11, 12, 14, 15, 16, 17, 18, 19) Using Gaussian Filter Function. (2012), IJINS.
[15] Sobrino J.A., *et al.*, 90 (2004). Land surface temperature retrieval from LANDSAT TM 5. Remote Sensing of Environment, 90 (2004), pp. 434-440
[16] Sobrino J.A., *et al.*, (1996): Multi-channel and multi-angle algorithms for estimating sea and land surface temperature with ATSR data. *Int. J. Remote Sens.,* pp. 2089– 2114.
[17] Sobrino J. A., *et al.*, (1993). Theoretical split-window algorithms for determining the actual surface temperature. Il Nuovo Cimento C.
[18] Sobrino J.A., Raissouni N., (2000): Toward remote sensing methods for land cover dynamic monitoring: Application to Morocco. *Int. J. Remote Sens.,* pp. 353–366.
[19] Tang B., *et al.*, (2008). Generalized Split-Window Algorithm for Estimate of Land Surface Temperature from Chinese Geostationary FengYun Meteorological Satellite (FY-2C) Data. Sensors.
[20] Wang H., *et al.*, (2019). A Split Window Algorithm for Retrieving Land Surface Temperature from FY-3D MERSI-2 Data. Remote Sens.
[21] Wan Z., *et al.*, 83 (2002). Validation of the land-surface temperature products retrieved from Terra Moderate Resolution Imaging Spectroradiometer data. Remote Sensing of Environment, pp. 163-180
[22] Ye X., *et al.*, (2022). Split-Window Algorithm for Land Surface Temperature Retrieval From Landsat-9 Remote Sensing Images. IEEE.
[23] Zhang S., *et al.*, (2019). Improvement of Split-Window Algorithm for Land Surface Temperature Retrieval from Sentinel-3A SLSTR Data Over Barren Surfaces Using ASTER GED Product. Remote Sens.
[24] Zhou L., *et al.*, (2019) An Overview of the Science Performances and Calibration/Validation of Joint

Authors Profile

The authors have no conflicts of interest to declare

Nisrine Chekroun received the Bachelor degree in Physics, and Telecommunication Systems and Networks Engineering Diploma from Abdelmalek Essaadi University (National School for Applied Sciences) of Tetuan, Morocco, in 2017. Currently, she is a PhD student at Telecommunications and Embedded Systems Department, and member of Remote Sensing & GIS group.

Naoufal Raissouni received the M.S., and Ph.D. degrees in physics from the University of Valencia, Spain, in 1997, and 1999, respectively. He has been a Professor of physics and remote sensing at the National Engineering School for Applied Sciences of the University Abdelmalek Essaadi (UAE) of Tetuan, since 2003. He is also heading the Innovation & Telecoms Engineering research group at the UAE, responsible of the Remote Sensing & GIS group. His research interests include atmospheric correction in visible and infrared domains, the retrieval of emissivity and surface temperature from satellite image, huge remote sensing computations, Mobile GIS, Adhoc networks and the development of remote sensing methods for land cover dynamic monitoring.

Mohammed Lahraoua is a Prossor Searcher at FSJES Abdelmalek Essaadi University of Tangier. A member GéoTéCa group

Fatima Zahrae Rhziel is a Ph.D. candidate in telecommunication and remote sensing at Abdelmalek Essaadi University, The national school of applied Sciences, Tetouan, Morocco. She received her M.S. degree in signal processing and machine learning from National School of Applied Science (ENSA), Tetouan, Morocco, in 2019. She completed her B.Sc. in Physics from Sidi Mohammed Ben Abdellah University, Fes, Morocco, in 2017.
Rhziel is a member of the remote sensing & GIS research group and her research interests lie in the field of remote sensing, land surface temperature and thermal infrared sensors. Specifically, she is interested in the use of remote sensing data and techniques for monitoring land surface temperature and assessing thermal infrared sensors.

Assaad El Makhloufi received the Bachelor degree in Physics, and Telecommunication Systems and Networks Engineering Diploma from Abdelmalek Essaadi University (National School for Applied Sciences) of Tetuan, Morocco, in 2017. Currently, he is a Dr. Eng. at Telecommunications and Embedded Systems Department, and member of Remote Sensing & GIS group.